ARTICLE · OPEN

Check for updates

Soft, full Wheatstone bridge 3D pressure sensors for cardiovascular monitoring

Yoonseok Park [1 ✉], Haiwen Luan [2], Kyeongha Kwon [3], Ted S. Chung[4], Seyong Oh[5], Jae-Young Yoo[6], Gooyoon Chung [1], Junha Kim[1], Suhyeon Kim[1], Sung Soo Kwak [7], Junhwan Choi[8], Hoang-Phuong Phan [9], Seonggwang Yoo [10], Hyoyoung Jeong [11], Jaeho Shin[7], Sang Min Won [12], Hong-Joon Yoon[13], Yei Hwan Jung[14] and John A. Rogers [10,15 ✉]

Variations in parameters associated with the ambient environment can introduce noise in soft, body-worn sensors. For example, many piezoresistive pressure sensors exhibit a high degree of sensitivity to fluctuations in temperature, thereby requiring active compensation strategies. The research presented here addresses this challenge with a multilayered 3D microsystem design that integrates four piezoresistive sensors in a full-Wheatstone bridge configuration. An optimized layout of the sensors relative to the neutral mechanical plane leads to both an insensitivity to temperature and an increased sensitivity to pressure, relative to previously reported devices that rely on similar operating principles. Integrating this 3D pressure sensor into a soft, flexible electronics platform yields a system capable of real-time, wireless measurements from the surface of the skin. Placement above the radial and carotid arteries yields high-quality waveforms associated with pulsatile blood flow, with quantitative correlations to blood pressure. The results establish the materials and engineering aspects of a technology with broad potential in remote health monitoring.

INTRODUCTION

Cardiovascular diseases represent leading causes of mortality, emphasizing the necessity for effective and continuous monitoring systems to facilitate proactive management of these conditions[1,2]. Most existing approaches rely on wired systems confined to use in hospitals[3]. Despite the development of advanced technologies that overcome some of these limitations[4–7], challenges remain in monitoring of dynamic processes such as time-dependent pressures associated with pulsatile blood flow[8,9], in ways that are insensitive to variations in temperature and other characteristics of the ambient.

The research summarized here contributes to this field through the introduction of a three-dimensional (3D) piezoresistive sensor that automatically compensates for temperature variations by use of a Wheatstone bridge architecture and an optimized mechanical layout. Combining these sensors with Bluetooth wireless communication technology in systems that exploit the design principles of soft electronics[9–12], yields capabilities in continuous measurements of hemodynamic properties, including correlations to blood pressure, in skin-interfaced platforms that mount gently on the wrist or neck. The result can support monitoring in home settings with minimal disruption to normal daily activities. The following presents all of the materials and engineering details associated with these devices and illustrates their use in monitoring of cardiovascular conditions, with quantitative comparisons to standard methods.

RESULTS

Figure 1a shows an exploded view schematic illustration of a lithographically fabricated multilayer stack that includes (i) a layer of polyimide (PI; PI2545, HD MicroSystems; 4 µm in thickness) on the bottom as a support, (ii) a network of interconnects and two resistive strain gauges connected in series (a trace of Cr/Au in a serpentine geometry; width 3 µm; thickness 5/45 nm; resistance 520 ohms), (iii) a layer of PI (4 µm in thickness) as a middle separating layer, (iv) a network of interconnects and two strain gauges (a trace of Cr/Au; width 3 µm; thickness 5/50 nm; resistance, 480 ohms), and (v) a layer of PI (4 µm in thickness) on the top as encapsulation. Mechanically guided assembly[13–18] transforms a microfabricated 2D multilayer stack with this layout into a 3D Multiple strain gauge Integrated smart Sensor (3MIS) (Fig. 1b, Supplementary Fig. 1). The two sets of gold traces located on the four legs of the resulting table-shaped 3D structure have similar resistance (~500 ohms). This layout defines a Wheatstone full bridge circuit to convert the resistance change associated with

[1]Department of Advanced Materials Engineering for Information and Electronics, Integrated Education Institute for Frontier Science & Technology (BK21 Four), Kyung Hee University, Yongin-si, Gyeonggi-do 17104, Republic of Korea. [2]Department of Mechanical and Aerospace Engineering, University of California San Diego, La Jolla, CA 92093, USA. [3]School of Electrical Engineering, Korea Advanced Institute of Science and Technology, Daejeon, Republic of Korea. [4]Department of Mechanical Engineering, Columbia University, New York, NY, USA. [5]Division of Electrical Engineering, Hanyang University ERICA, Ansan 15588, Republic of Korea. [6] Department of Semiconductor Convergence Engineering, Sungkyunkwan University, Suwon, Republic of Korea. [7]Biomedical Research Division, Korea Institute of Science and Technology, Seoul 02792, Republic of Korea. [8]Department of Chemical Engineering, Dankook University, Yongin, Gyeonggi-do 16890, Republic of Korea. [9]School of Mechanical and Manufacturing Engineering, Tyree Institute of Health Engineering, University of New South Wales, Sydney, NSW 2052, Australia. [10]Querrey Simpson Institute for Bioelectronics, Northwestern University Evanston, Evanston, IL 60208, USA. [11]Department of Electrical and Computer Engineering, University of California Davis, Davis, CA 95616, USA. [12]Department of Electrical and Computer Engineering, Sungkyunkwan University, 2066, Seobu-ro, Jangan-gu, Suwon-si, Gyeonggi-do 16419, Republic of Korea. [13]Department of Electronic Engineering, Gachon University, Seongnam-si, Gyeonggi-do 13120, Republic of Korea. [14]Department of Electronic Engineering, Hanyang University, Seoul, Republic of Korea. [15]Department of Materials Science and Engineering, Biomedical Engineering, Neurological Surgery, Chemistry, Mechanical Engineering, Electrical Engineering and Computer Science Simpson Querrey Institute and Feinberg Medical School, Center for Bio-Integrated Electronics, Northwestern University Evanston, Evanston, IL 60208, USA. ✉email: yoonseok.park@khu.ac.kr; jrogers@northwestern.edu
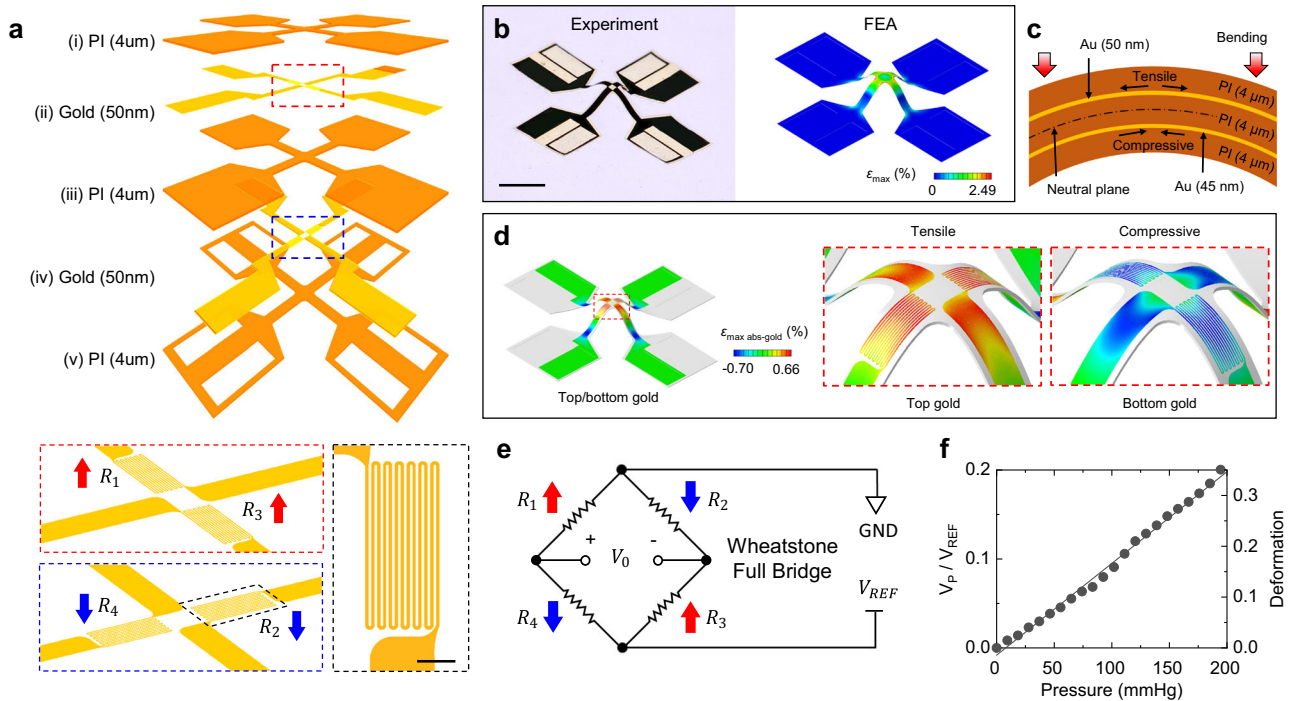
Fig. 1 Multilayer metal-PI 3D structures as strain gauges in a Wheatstone full-bridge configuration. a Exploded view schematic illustration of a 2D precursor that consists of top, middle, and bottom films of polyimide (PI), with two layers that define serpentine structures of gold as piezoresistive strain gauges (~500 Ω). Scale bar, 60 μm. **b** Experimental image and FEA prediction of the 3D structure formed by compressive buckling. Scale bar, 1 mm. **c** Cross-sectional schematic illustration of the 3D structure under bending. Gold layers on different sides of the mechanical neutral plane experience tensile and compressive strains, respectively. **d** FEA predictions of the strain distributions for both gold layers. The top strain gauges are under tension and the bottom ones are under compression. **e** Circuit diagram of the sensor. The four strain gauges (R_1, R_2, R_3, R_4) form a Wheatstone full bridge. **f** Fractional change in V_P/V_{ref} values of a 3D pressure sensor as a function of normal pressure loading.

the strain sensors (R_1, R_2, R_3, and R_4) into a voltage change. The bridge circuit has two parallel resistive branches that act as voltage dividers for the reference voltage (V_{REF}; 3.3 V). The voltage output of the bridge (V_O) is 0 V when the bridge is balanced (i.e., $\frac{R_1}{R_1+R_4} = \frac{R_2}{R_2+R_3}$), according to the following equation.

$$V_O = \left(\frac{R_1}{R_1 + R_4} - \frac{R_2}{R_2 + R_3} \right) V_{REF} \qquad (1)$$

Application of normal pressure onto the 3MIS induces tensile and compressive deformations of the metal traces placed above and below the mechanical neutral plane. The result is an increase (R_1 and R_3) and decrease (R_2 and R_4) in the resistances of the metal traces (Fig. 1c–e). The circuit increases the bridge output following changes in the resistance of each strain sensor. A subsequent amplifier (AMP) amplifies this output with a fixed gain of 6 *V/V*, resulting in an AMP output voltage (V_P) of $V_P = 6V_O$.

Figure 1f shows a linear correlation (*pressure = 400 × V_p/V_{ref}*) between the AMP output voltage change (V_P/V_{REF}) and the applied pressure, measured while simultaneously recording the associated deformation using a force measurement system (FMS; motorized force tester, Mark-10, Supplementary Fig. 2). The sensors exhibit reliable values under different loading pressures (Supplementary Fig. 3). The designs and material selections of the 3MIS optimize for linear response in a relatively low-pressure range of interest for measurements of superficial pressure (0–200 mmHg) on the skin associated with pulsatile blood flow.

Encapsulating a 3MIS in a silicone elastomer (Ecoflex 00-30) with an acrylic ring as a frame, with serpentine PI layers (SPL) ensures mechanically stable operation and resistance to shear stresses. The dimensions of the 3MIS and the assembled sensor are 1.2 mm × 0.5 mm and 2.8 mm × 875 μm, respectively (radius ×

thickness, Fig. 2a). Placing the assembled sensor on a layer of conductive epoxy (8331 Silver Adhesive; MG Chemicals) on a flexible printed circuit board (PCB) forms an electrical connection. Piezoresistive strain sensors of this general type[19–21] respond both to changes in deformation and temperature. The quarter-bridge (QB) configuration shown in Fig. 2b exploits one microfabricated piezoresistive sensor (R_4) and 3 commercial resistors (R_c 500 ohm, SMD 0201 thick film resistor). The changes in the resistance of R_4 and R_c with temperature are different, such that V_P varies with ambient temperature in the absence of deformation. By comparison, four microfabricated piezoresistive sensors in a full-bridge (FB) configuration exhibit identical changes in resistance with temperature, thus eliminating significant variations for temperatures between 25 and 40 °C (Fig. 2c). The result in Fig. 2d compares the pressure responses of devices with the FB and QB designs. The sensitivity of the FB case (slope = 0.0031) is three times higher than that of the QB (slope = 0.009). Following Eq. (1), when normal pressure is applied to the 3MIS sensor, the value of R_1 increases due to tensile deformation. In contrast, the value of R_2 decreases due to compressive deformations. Both responses depend linearly on pressure ($R^2 = 0.995$) over a range of 200 mmHg. These comparisons of sensitivity to pressure and temperature highlight the advantages of the FB design in the 3MIS sensor. Measurements to explore the thermal effects involve both sensors in an ambient condition (Supplementary Fig. 4) and on a hot plate at a temperature of 30 °C, while applying pressure (100 mmHg) using a metal disc at room temperature (23 °C) (Fig. 2e). Cycling between these two temperatures induces thermal drifts (QB sensor requires more than 30 s for recovery) that lead to hysteresis and associated inaccuracies in measurements of pressure with the QB design (Fig. 2f, g).
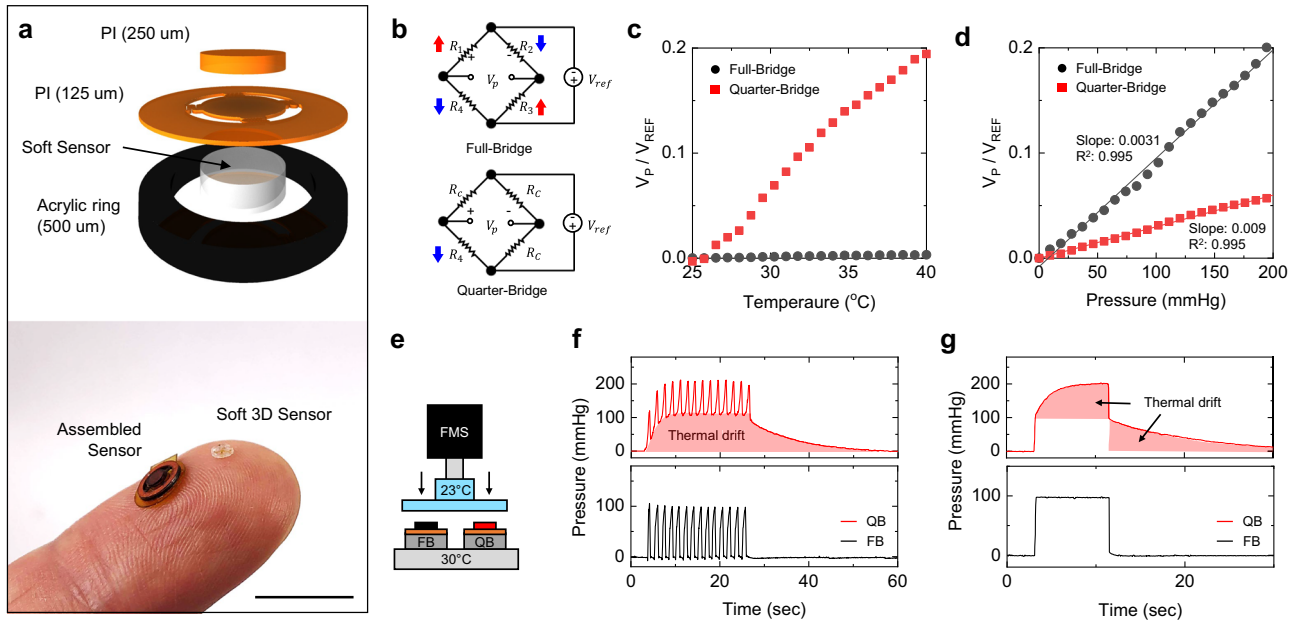
Fig. 2 Temperature response and pressure sensitivity of 3D pressure sensors with Wheatstone full-bridge and quarter-bridge designs. **a** Exploded view schematic illustration and photograph of a 3D pressure sensor. Scale bar, 10 mm. **b** Circuit diagram of the full-bridge (FB) and quarter-bridge (QB) sensors; the FB consists of four strain gauges (R_1, R_2, R_3, R_4) and the QB consists of one strain gauge (R_4) and three temperature-independent commercial resistors (R_c). **c** Fractional change in ADC values as a function of temperature for the FB and QB sensors. **d** Fractional change in ADC values as a function of normal pressure loading for the FB and QB sensors. **e** Schematic illustration of a benchtop setup for testing the effects of temperature on the measurements. Force measurement stands for dynamic mechanical analysis. **f** Fractional change in pressure values during 12 repeated cycles of pressure loading and unloading within 60 s. **g** Fractional change in pressure values during constant pressure loading for 10 s.

Tests of the response under shear stresses validate design choices to ensure responses only to normal pressure. Here, the geometry of the SPL is important. Tests using a motorized force tester and modeling by FEA summarized in Fig. 3a indicate an insensitivity of the encapsulated 3MIS system to shear stresses. Specifically, the application of force (0.1 N) against the side of the PI cylinder placed on top of the sensor oriented along the n-axis (Fig. 3b) and the m-axis (Fig. 3c) leads to stresses concentrated near the periphery of the interface between the assembled sensor and the bottom substrate. Stresses around the 3D sensing structure are negligible. In experiments to validate the enhanced mechanical stability of the pressure sensor induced by the SPL, a motorized force tester applies a normal load onto the side of the sensors (Supplementary Fig. 5). In Fig. 3d, the sensor without the SPL malfunctions under shear stress. In contrast, the sensor with the SPL is stable under a shear stress of 0.1 N. After removing the shear stress, the sensor recovers its original shape and returns a reading of 0 mmHg (Fig. 3e). In separate tests using the FMS to apply normal pressures from 0 to 100 mmHg indicates stable operation over 1000 cycles (Fig. 3f).

The 3MIS pressure sensors reported have optimized dynamic range, accuracy, and time response for measurements of variations of superficial pressures (less than 100 mmHg) associated with blood flow through near-surface blood vessels[22,23]. The recorded pressure waveforms provide insights into cardiovascular health through measurements of heart rate and, with appropriate calibration, blood pressure. Elastomeric tubing embedded in artificial skin and pumped with water using a system to simulate pulsatile hemodynamics[24] serves as the basis for benchtop validation, as shown in Fig. 4a. Specifically, this setup consists of a pulse generator, two water cylinders, and tubing to simulate the heart, blood supply, and blood vessels, respectively. The phantom skin consists of a silicone-based elastomer (Young's modulus $E = 60$ kPa for Ecoflex 00-30). The 3MIS rests on the surface of the artificial skin above the artificial blood vessel, which consists of a

different silicone elastomer formulation ($E = \sim 2.0$ MPa) with outer and inner diameters of 4.5 mm and 3.0 mm, respectively (Fig. 4b). A metal post rests on the top of the sensor to provide a fixed downward pressure of ~35 mmHg. Transformation of pressures measured with the 3MIS to the pressures produced by the artificial heart system exploits a dimensionless factor k that depends on the mechanical properties of the phantom skin[25] and experimental data, according to the following equation;

$$BP = kP_{sensor} \qquad (2)$$

The coefficient of proportionality k is experimentally determined to 2.1. Figure 4c shows the results of this transformation for the case of data recorded at four different pulse frequencies (50 Hz, 70 Hz, 90 Hz, 110 Hz) over a period of 120 s. A reference pressure sensor in the simulator system and the 3MIS on the skin phantom measure changes in pressure (Fig. 4c, d). The normalized waveforms recorded in this manner show excellent agreement for these four different pulse frequencies (Fig. 4e).

A complete wireless system that integrates this technology includes a flexible printed circuit board (PCB) with the following constituent layers and components: silicone encapsulation, a coin cell battery (CR1229), a 3MIS pressure sensor (R_1, R_2, R_3, R_4), an NTC temperature sensor (R_T) and other standard electronics (Fig. 5a, b). The substrate is a thin, flexible copper-clad polyimide (PI) film (AP8535R, Pyralux) processed with a laser cutting tool (ProtoLaser U4, LPKF) to yield conductive traces that interconnect a Bluetooth low energy (BLE) system on a chip and Wheatstone bridge circuits configured with the NTC (Fig. 5c). The thin, flexible and lightweight construction yields a soft, comfortable interface to the skin at the locations of the radial and carotid arteries (Fig. 5d, f). Data collected with this system yield clear pulse waveforms with features that correspond to expected systolic peaks (SP) and diastolic peaks (DP) and notches (Fig. 5e, g).
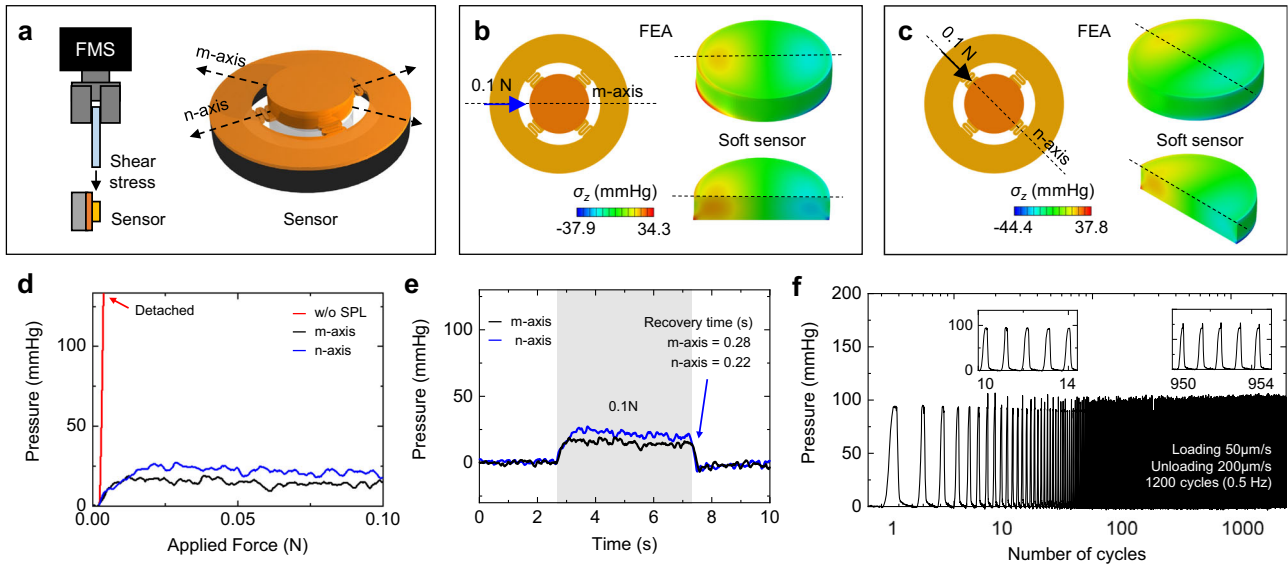
Fig. 3 Tests of the mechanical integrity of the 3D pressure sensor. a Schematic illustration of a benchtop setup to test responses to shear stress. Deformation states and stress distributions are determined by FEA as the sensor is subjected to increasing force along the m-axis (**b**) and n-axis (**c**). **d** Fractional change in ADC values as a function of shear force. SPL stands for the serpentine PI layer. **e** Fractional change in ADC values during 5.5 s of 0.1 N of shear force. **f** Fractional change of ADC at different stages of fatigue testing at loading speeds of 50 and 200 μm/s (loading and unloading) over 1000 cycles.

Practical studies involve normal healthy subjects. A reference measurement set-up (Finapress® NOVA) mounts on a finger and at the chest for recordings captured simultaneously with a 3MIS device held at the radial artery with an adjustable wristband (Fig. 6a). Adhesive tape on the backside of the device provides secure attachment on the radial artery. The wristband applies a stable pressure of ~40 mmHg on the pressure sensor and ensures adhesion between the device and skin (Supplementary Fig. 6, Supplementary Video 1). The value of k depends on the skin modulus. For the sensor applied onto the radial artery, the k value is 2.1. A calibration process enables precise measurements for individual subjects. In Fig. 6b, experimentally acquired k from the 3MIS and reference system (subject 1: 2.2, subject 2: 2.1, subject 3: 2.15) transforms P_{sensor} to BP. The mean arterial pressure (MAP) serves as a metric to compare results from the 3MIS and reference system, according to,

$$\mathrm{MAP} = \mathrm{DP} + \frac{1}{3(\mathrm{SP} - \mathrm{DP})} \qquad (3)$$

The experiments involve recording cardiovascular information for 10 min as the subject performs a Valsalva maneuver (a forceful attempt of exhalation against a closed airway) for 30 s, a breath hold for 90 s and an immersion of the opposite hand into ice water for 70 s (Supplementary Fig. 7). A sequence of rapid changes in preload and after load stress causes changes in heart rate (HR) and MAP due to an increase in intrathoracic pressure appear, as expected, in the data collected from these two different measurement systems (Fig. 6c). Expected changes also appear from elevations in MAP and HR due to breath holding and elevations in MAP and decreases in HR due to ice water immersion. MAP, HR, SP and DP collected by the reference and 3MIS devices from three healthy subjects show excellent agreement in the Bland-Altman plot (Fig. 6d, e). The system performs pressure measurements at a 100 Hz sampling rate and transmits an averaged pressure value every 0.25 s (4 Hz) to a smart device. The replaceable battery for these measurements (CR 1220; 3 V, 37 mA h) has an expected lifetime of 30 days.

DISCUSSION
In this research, we developed a soft, 3D piezoresistive sensor system for continuous monitoring of pressure, with a focus on applications in healthcare. The designs offer advantages in sensitivity to pressure and insensitivity to temperature compared to previously reported devices that use similar sensing principles. The key feature is a full Wheatstone bridge configuration that eliminates the need to calibrate the sensor for variations in temperature. This design also improves the sensitivity for measurements of pressure relevant to cardiovascular conditions.

The system exhibits a linear response, free of hysteresis with optimized performance in measurements of superficial pressure on the skin. Soft elastomeric polymers for encapsulation and rigid framing structures ensure comfortable, but robust interfaces to the body with sensitivity only to normal pressures. A system level embodiment integrates the sensor into a flexible PCB platform that supports wireless communication via BLE technology. Practical studies involving normal healthy subjects validate the performance of the sensor system, showing good agreement with a reference standard measurement setup for capturing cardiovascular information such as MAP and HR. These results suggest the potential for broad applications in healthcare management, through early interventions and personalized care.

METHODS
Fabrication of the 3MIS sensor
Preparation of 2D precursor structures began with spin coating (3000 rpm for 30 s) and curing (180 °C for 2 min) a thin layer of poly(methyl methacrylate) (PMMA) on a clean glass slide, followed by spin coating and fully curing (260 °C for 1 h) a layer of PI (4 μm; PI-2545, HD MicroSystems). Electron beam evaporation formed thin films of chrome (Cr, 5 nm) and gold (Au, 45 nm) on the PI. Photolithography and lift-off processes yielded bottom serpentine gold patterns in these thin metal films. Spin coating and curing another layer of PI (4 μm) created an insulating polyimide film on these conductive features. Electron beam evaporation formed thin films of Cr and Au (5 nm and 50 nm) ona PI film; top gold
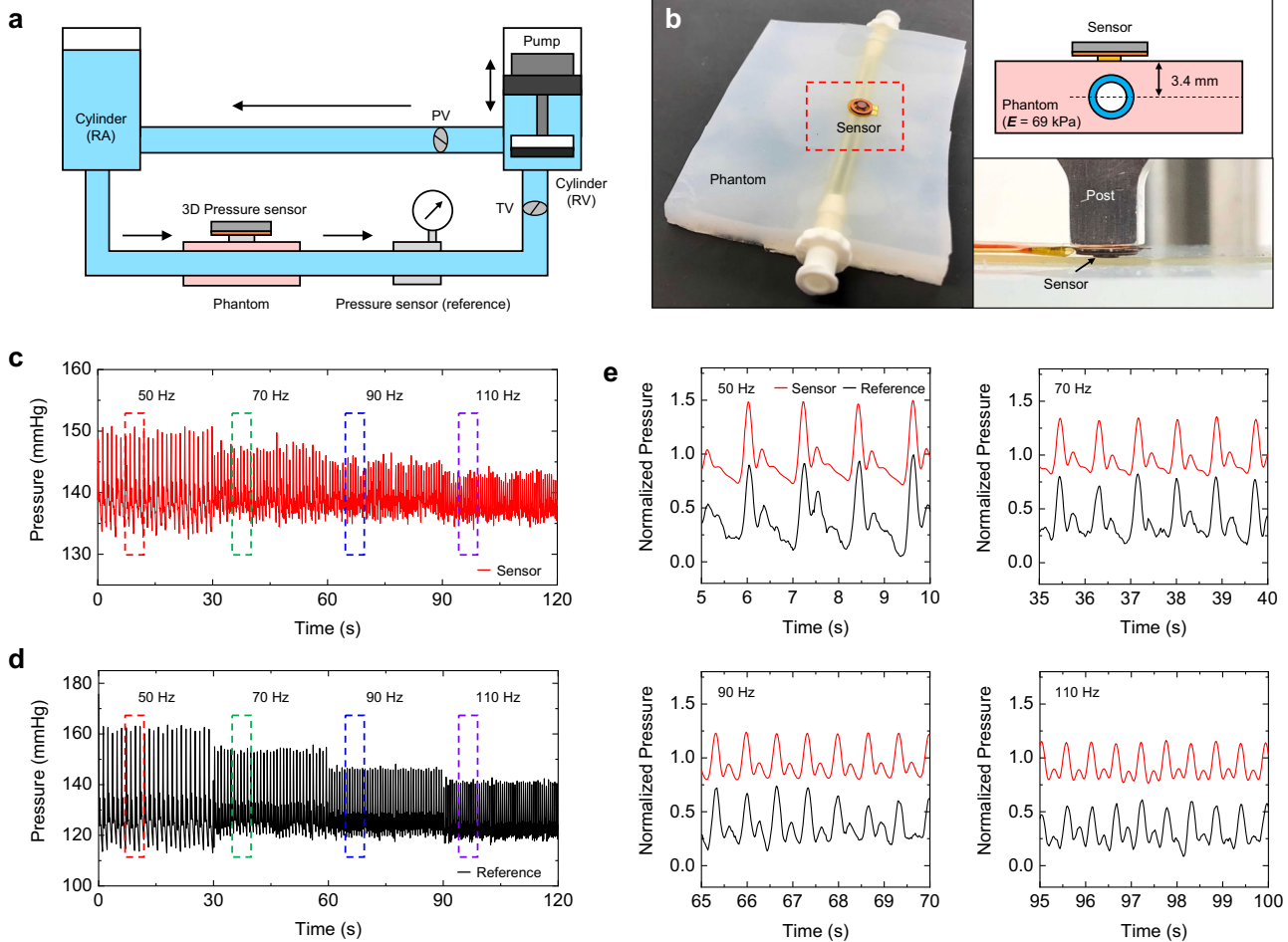
Fig. 4 Uses of a 3D pressure sensor for measurements on the surface of a phantom skin and artery connected to a cardiac simulator. **a** Schematic diagram of the experimental setup, which consists of a pulse generator, two cylinders; right atrium (RA), right ventricle (RV) and tubing to simulate the heart, blood supply, and blood vessels, respectively. **b** Photographs and schematic illustration of a phantom skin and artery made from silicone-based elastomers (Young's modulus, 60 kPa for Ecoflex 00-30, and 2 MPa for silicon rubber) with a 3MIS sensor placed on the surface. **c** Continuous superficial pressure as a function of increasing pulse frequencies over a period of 120 s. **d** Pressure measured by a commercial sensor at the same frequencies over a period of 120 s. **e** Normalized pulse waveforms recorded by the 3MIS and reference sensor with varying amplitudes and pulse rates.

serpentine patterns were prepared by photolithography. Spin coating and curing the final layer of PI (4 μm) created an insulating top film. A thin layer of copper (Cu, 100 nm) deposited on the PI by sputtering and patterned by photolithography and wet etching served as a hard mask for oxygen plasma etching (220 mT, 200 W, 120 min) of the exposed regions of the PI. Immersion in acetone overnight dissolved the underlying PMMA, thereby allowing the structures to be retrieved from the glass slide. Transferring this 2D precursor onto the surface of a poly(dimethylsiloxane) stamp and again onto the surface of a water-soluble tape prepared the system for the geometry transformation. This process involved laminating the 2D precursor/poly(vinyl alcohol) tape on top of an elastomer substrate prestretched to an equal biaxial strain of 30%. Dissolving the PVA tape with water and releasing the pre-stretch transformed the 2D precursors into 3D mesostructures, with the rectangular-shaped contact areas as bonding sites. Encapsulating the 3D structure in Ecoflex 00-30 (Smooth-On, PA, USA) using a mold (diameter, 3 mm; height, 500 μm) completed the fabrication. Placing the encapsulated 3D structures on an FPCB allowed for electrical interconnection using a conductive epoxy. A ring-shaped structure of acrylic and PI layers stacked on the 3D sensor provided mechanical stability. Illustrations in Supplementary Fig. 1 feature each step in detail.

Fabrication of the electronics
The FPCB design layouts were created using EAGLE CAD version 9 (Autodesk). To fabricate the FPCB, a sheet of FPCB with a thickness of 12 μm for the top and bottom copper layers and 25 μm for the middle PI layer (AP7164R, DuPont) was patterned into the required shapes using an ultraviolet laser cutter (LPKF U4). The 3D pressure sensor, along with various surface-mount components including the BLE SoC (nRF52832, Nordic Semiconductor), BLE antenna (2450AT18A100, Johanson Technology Inc.), AMP (INA333, Texas Instruments), reference resistors (RMCF0201FT, Stackpole Electronics Inc.), and temperature sensor components (NTC; NCP03XH, Murata), were joined to the FPCB using solder paste (Chip Quik TS391LT) and reflowed using a heat gun (AOYUE Int866). The temperature sensor components were chosen for their high accuracy in resistance and long-term stability.
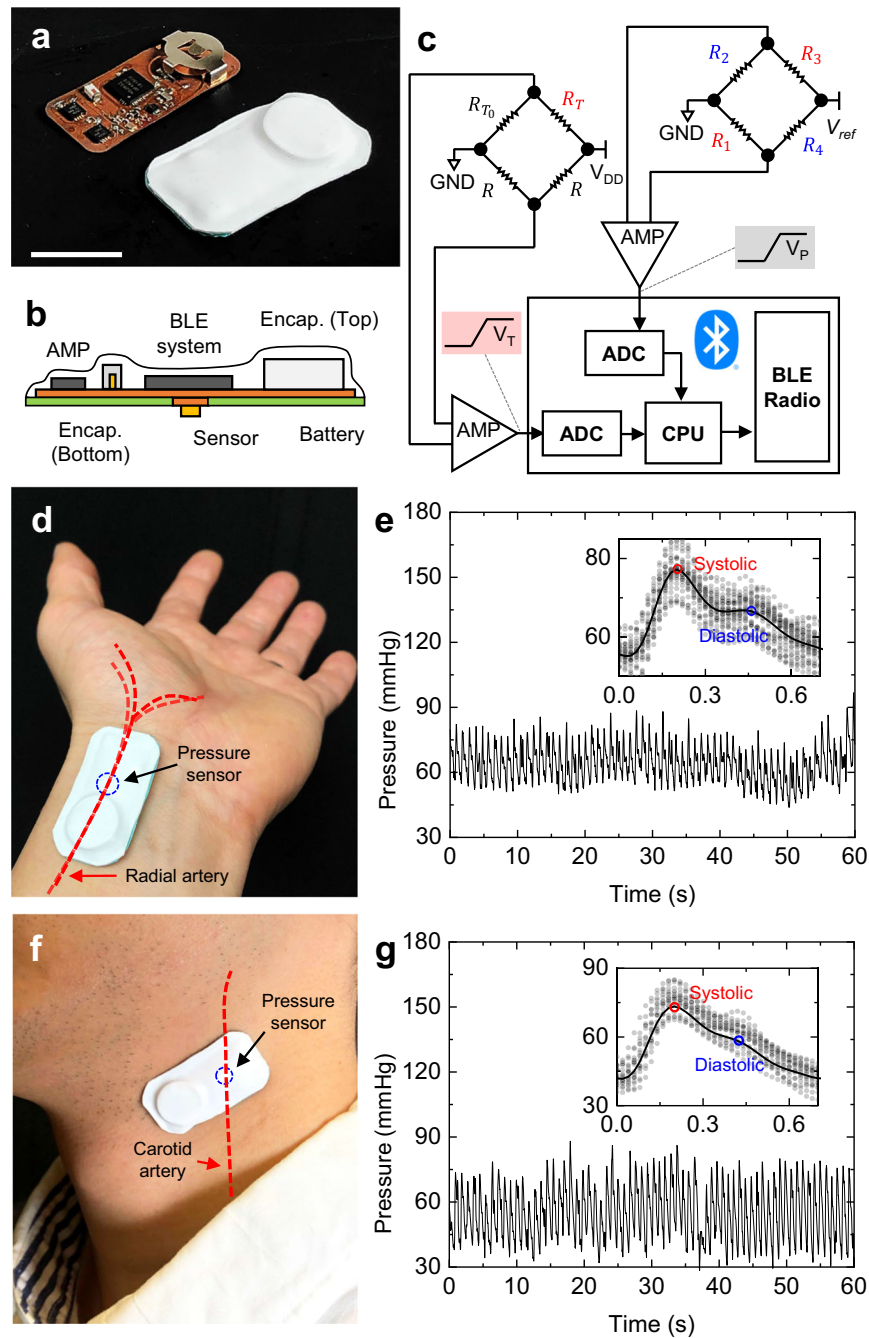
Fig. 5 Evaluations of a wireless pressure sensing system based on a 3MIS, mounted on the skin at the radial and carotid arteries, respectively. a Photograph of a sensor without (left) and with encapsulation (right). Scale bar, 20 mm. **b** Schematic cross-sectional illustration of the system. **c** Circuit and block diagrams. **d** Photographs of a system mounted on the radial artery. **e** Continuous superficial pressure and overlaid waveforms of pulsatile blood flow with an indication of diastolic and systolic peaks (inset) from the radial artery. **f** Photographs of a system mounted on the carotid artery. **g** Continuous superficial pressure and overlaid waveforms of pulsatile blood flow with an indication of diastolic and systolic peaks (inset) from the carotid artery.

Assembly of wireless systems

To begin the encapsulation process, a soft silicone film (SILBIONE RTV 4420; A&B, Bluestar Silicones) was spin-cast at 250 rpm and thermally cured at 100 °C in an oven for 20 min onto a glass slide, forming the bottom layer. Aluminum molds with specific geometries, defined by 3D computer-aided design drawings generated using SOLIDWORKS 2020, were created using a milling machine (Roland MDX-540). The capping membrane was formed by casting a liquid precursor of a silicone polymer (SILBIONE RTV 4420; A&B, Bluestar Silicones) and thermally curing it in an oven at

100 °C for 20 min. A CO_2 laser cutting process (Universal Laser Systems, Inc.) created an opening on the capping layer for the pressure sensor and a replaceable battery. A manual alignment process aligned the openings on the capping layer with the pressure sensor and battery on the FPCB.

Characterizing the pressure sensors

Changes in resistance and calibrated pressure readings from the 3D sensor as a function of pressure applied using an FMS (RSA-G2
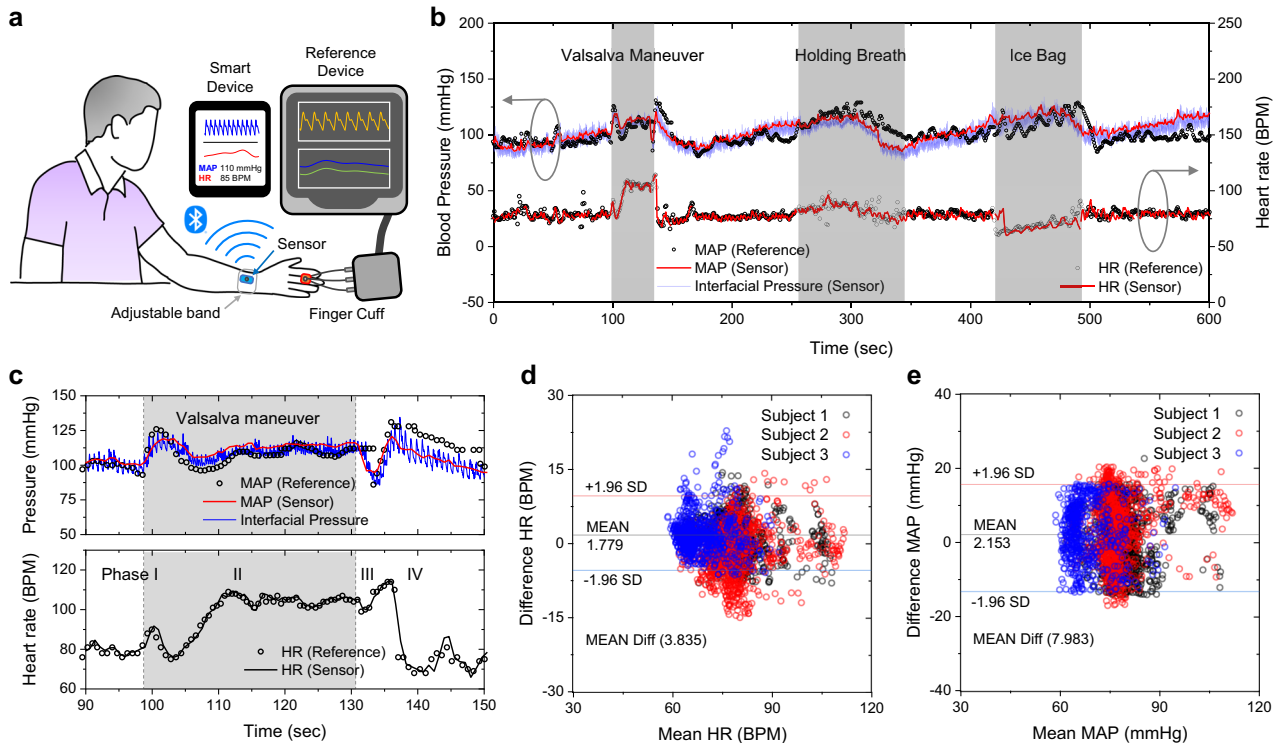
Fig. 6   Evaluations of a wireless pressure sensor mounted on the skin at the radial artery and a reference device mounted on the finger of healthy volunteers. a Illustration of monitoring cardiovascular information from a human subject with the reference device and 3MIS system. **b** Continuous measurement of blood pressure and heart rate. The subject performs a Valsalva maneuvre for 30 s, a breath hold for 90 s and immersion of the opposite hand into ice water for 70 s. **c** Magnified view of cardiovascular information during the Valsalva maneuver from (**b**). **d** Bland–Altman plot comparing HR from the 3MIS system and reference device. **e** Bland–Altman plot comparing MAP from the 3MIS system and reference device.

Solids Analyzer, TA Instruments) were stored through wireless communication.

Characterizing the temperature-independent property of sensors

QB sensor and FB (compensated 0 mmHg at 30 °C) sensors were placed on the hot plate (30 °C) for 10 min and the pressure of QB sensor is compensated as 0 mmHg. Calibrated pressure from both sensors was stored through a digital multimeter while FMS applied 100 mmHg pressure using metal disk (Room temperature, 23 °C).

Feasibility tests of the wireless devices

The studies involved a volunteer (subject 1: male, 29 years old, subject 2: male, 38 years old, subject 3: male, 40 years old) with a pressure sensor placed on the radial artery. While lying on a medical bed, pressures were measured and compared with reference measurement set-up. The same volunteer performed various activities (Valsalva maneuver and holding breath, and ice-bag) with the 3MIS.

Processing sensor data

To process the sensor data, calculated pressure values were transferred from the sensor to smart devices using Bluetooth wireless system. The Python scipy.signal.find_peaks algorithm was used to find the systolic and diastolic peaks.

Finite element analysis

3D finite element analysis (FEA) was performed in the software package Abaqus to capture the nonlinear postbuckling behaviors

of 2D precursor structures, and to analyze the mechanical performance of the 3D structures and the wireless electronic device. Linear buckling analysis was performed for the 2D precursor structure to determine the critical buckling strain and corresponding buckling mode. Initial geometric imperfections according to the buckling mode were implemented in postbuckling analysis. The deformed configurations and stress/strain distributions of the 3D mesoscale structure were obtained from FEA. Eight-node solid elements and four-node shell elements were chosen for the silicone materials (e.g., assembly substrate, encapsulation, etc.) and the 2D precursor structures (i.e., PI thin films with metal traces), based on the design specifics. The Mooney-Rivlin strain energy potential model was used for elastomeric materials with hyperelastic behavior. PDMS (10:1) was modeled as incompressible, with an elastic modulus $E_{PDMS} = 1.8$ MPa. Ecoflex 00-30 was modeled as incompressible, with an elastic modulus $E_{Ecoflex} = 60$ kPa. PI and PMMA were modeled with linear elastic behavior, with an elastic modulus of $E_{PI} = 2.5$ GPa and a Poisson's ratio of $v_{PI} = 0.34$ for PI, and an elastic modulus of $E_{PMMA} = 3.1$ GPa and a Poisson's ratio of $v_{PMMA} = 0.37$ for PMMA, respectively. Metal materials, such as gold (Au) and copper (Cu), were modeled as elastoplastic (without hardening; yield strain chosen as 0.3%). The elastic modulus and Poisson's ratio are $E_{Au} = 78$ GPa and $v_{Au} = 0.44$ for Au and $E_{Cu} = 119$ GPa and $v_{Cu} = 0.34$ for Cu, respectively.

Clinical studies

This study was approved by Northwestern University's Institutional Review Board, under trial registration numbers STU00202449 and STU00212522. After informed consent from all participants, participants wore reference measurement set-up and the 3MIS

system was placed on the radial artery by trained research staff, and interface pressures through 3MIS were recorded.

DATA AVAILABILITY
Additional data related to this paper may be requested from the corresponding authors upon reasonable request.

REFERENCES
1. Sana, F. et al. Wearable devices for ambulatory cardiac monitoring: JACC state-of-the-art review. *J. Am. Coll. Cardiol.* **75**, 1582 (2020).
2. Bayoumy, K. et al. Smart wearable devices in cardiovascular care: where we are and how to move forward. *Nat. Rev. Cardiol.* **18**, 581–599 (2021).
3. Drew, B. J. et al. Practice standards for electrocardiographic monitoring in hospital settings. *Circulation* **110**, 2721–2746 (2004).
4. Kuehn, B. M. Telemedicine helps cardiologists extend their reach. *Circulation* **134**, 1189–1191 (2016).
5. Rha, J. Y. et al. What drives the use of wearable healthcare devices? A cross-country comparison between the US and Korea. **8**, https://doi.org/10.1177/20552076221120319 (2022).
6. Hobensack, M., Song, J., Scharp, D., Bowles, K. H. & Topaz, M. Machine learning applied to electronic health record data in home healthcare: a scoping review. *Int J. Med Inf.* **170**, 104978 (2023).
7. White, E. M., Wetle, T. F., Reddy, A. & Baier, R. R. Front-line nursing home staff experiences during the COVID-19 pandemic. *J. Am. Med Dir. Assoc.* **22**, 199–203 (2021).
8. Kim, J. et al. Soft wearable pressure sensors for beat-to-beat blood pressure monitoring. *Adv. Health. Mater.* **8**, 1900109 (2019).
9. Kwon, K. et al. An on-skin platform for wireless monitoring of flow rate, cumulative loss and temperature of sweat in real time. *Nat. Electron. 2021* **4**, 302–312 (2021).
10. Bandodkar, A. J., Jeang, W. J., Ghaffari, R. & Rogers, J. A. Wearable sensors for biochemical sweat analysis. *Annu. Rev. Anal. Chem.* **12**, 1–22 (2019).
11. Kwon, K. et al. Wireless, soft electronics for rapid, multisensor measurements of hydration levels in healthy and diseased skin. *Proc. Natl Acad. Sci. USA* **118**, e2020398118 (2021).
12. Shin, J. et al. Wireless, soft sensors of skin hydration with designs optimized for rapid, accurate diagnostics of dermatological health. *Adv. Health. Mater.* **12**, 2202021 (2023).
13. Kim, B. H. et al. Three-dimensional silicon electronic systems fabricated by compressive buckling process. *ACS Nano* **12**, 4164–4171 (2018).
14. Park, Y. et al. Three-dimensional, multifunctional neural interfaces for cortical spheroids and engineered assembloids. *Sci. Adv.* **7**, eabf9153 (2021).
15. Ning, X. et al. Mechanically active materials in three-dimensional mesostructures. *Sci. Adv.* **4**, eaat8313 (2018).
16. Xu, S. et al. Assembly of micro/nanomaterials into complex, three-dimensional a by compressive buckling. *Science* **347**, 154–159 (2015).
17. Wang, X. et al. Three-dimensional electronic scaffolds for monitoring and regulation of multifunctional hybrid tissues. *Extrem. Mech. Lett.* **35**, 1–9 (2020).
18. Park, Y., Chung, T. S., Lee, G. & Rogers, J. A. Materials chemistry of neural interface technologies and recent advances in three-dimensional systems. *Chem. Rev.* **122**, 5277–5316 (2022).
19. Park, Y. et al. Wireless, skin-interfaced sensors for compression therapy. *Sci. Adv.* **6**, 1–10 (2020).
20. Won, S. M. et al. Multimodal sensing with a three-dimensional piezoresistive structure. *ACS Nano* **13**, 10972–10979 (2019).
21. Kwak, J. W. et al. Wireless sensors for continuous, multimodal measurements at the skin interface with lower limb prostheses. *Sci. Transl. Med.* **12**, 4327 (2020).
22. Webb, R. C. et al. Epidermal devices for noninvasive, precise, and continuous mapping of macrovascular and microvascular blood flow. *Sci. Adv.* **1**, e1500701 (2015).
23. Chi, Y. W., Tseng, K. H., Li, R. & Pan, T. Comparison of piezoresistive sensor to Pico-Press® in in-vitro interface pressure measurement. *Phlebology* **33**, 315–320 (2018).
24. Kwon, K. et al. A battery-less wireless implant for the continuous monitoring of vascular pressure, flow rate and temperature. *Nat. Biomed. Eng. 2023* **3**, 1–14 (2023).
25. Li, S. et al. Measurement of blood pressure via a skin-mounted, non-invasive pressure sensor. *J. Appl. Mech. Trans.* **88**, 101008 (2021).

AUTHOR CONTRIBUTIONS
Y.P., H.L., and K.K. contributed equally to this work. Y.P. and J.A.R. conceived of the overall research goals and aims; Y.P., H.L., and J.A.R. performed the designs and engineering investigation of the sensor. Y.P., K.K., T.S.C., G.C., J.K., H.-P.P., and S.K. manufactured the sensors and wireless devices. K.K., S.Y., and S.S.K. designed the hardware for the wireless electronics platform. K.K., S.O., and J-.Y.Y. performed software design and software validation. H.L. performed mechanical modeling. Y.P., J.S., W.S.M., Y.J., and T.S.C. performed in vitro characterizations. Y.P., J.C., H.J., J-.Y.Y., J.S., H-J.Y., and T.S.C. performed clinical data collection and analysis. Y.P. and J.A.R. were responsible for original drafting of the manuscript and all authors assisted in critical editing and review of the final manuscript.

COMPETING INTERESTS
The authors declare no competing interests.

ADDITIONAL INFORMATION
Supplementary information The online version contains supplementary material available at https://doi.org/10.1038/s41528-024-00294-3.

Correspondence and requests for materials should be addressed to Yoonseok Park or John A. Rogers.

Reprints and permission information is available at http://www.nature.com/reprints

Publisher's note Springer Nature remains neutral with regard to jurisdictional claims in published maps and institutional affiliations.